Chinese Chemical Letters 34 (2023) 108564

Contents lists available at ScienceDirect

Chinese Chemical Letters

journal homepage: www.elsevier.com/locate/cclet

Red light-driven generation of reactive oxygen species for the targeted oxidation of glioma cells and thiols over covalent organic framework

Heng Wei[1], Xia Li[1], Fengwei Huang, Shujuan Wu, Huimin Ding, Qianxue Chen, Mingchang Li*, Xianjun Lang*

Renmin Hospital of Wuhan University, College of Chemistry and Molecular Sciences, Wuhan University, Wuhan 430072, China

ARTICLE INFO

Article history:
Received 8 January 2023
Revised 8 May 2023
Accepted 10 May 2023
Available online 12 May 2023

Keywords:
Reactive oxygen species
Covalent organic framework
Oxidation
Photodynamic therapy
Glioma cells

ABSTRACT

Reactive oxygen species (ROS) are essential for biological processes like cell signaling and chemical processes like organic oxidation. Moreover, the sufficient generation of ROS plays a significant role in targeted tumor treatments or oxidation of organics. Herein, a hydrazone-linked porphyrin covalent organic framework (Por-DETH-COF) is developed for red light-induced generation of ROS like singlet oxygen ($^1O_2$) or superoxide ($O_2^{\bullet-}$) to undertake different but targeted oxidations. First, $^1O_2$ is adopted in photodynamic therapy (PDT) for the oxidation of glioma cells. The PDT efficiency of Por-DETH-COF on the apoptosis of glioma cells is explored through flow cytometry and western blot assay. The apoptosis rate of glioma cells significantly increases over Por-DETH-COF under 660 nm red light illumination, suggestive of the potency of $^1O_2$. Second, $O_2^{\bullet-}$ is employed for the targeted oxidation of thiols. A series of thiols could be efficiently oxidized to corresponding disulfides over Por-DETH-COF under 660 nm red light illumination, indicative of the significance of $O_2^{\bullet-}$. This work highlights the potential of covalent organic frameworks in generating ROS for precise medical applications of complex chemical environments.

Covalent organic frameworks (COFs) are an emerging type of porous organic materials with large specific surface areas, high crystallinity, low density, and good stability [1–6]. Besides, COFs, with excellent biocompatibility, have displayed enormous potential in biomedical applications [7–11]. Moreover, the exceptional light-harvesting capability and adjustable bandgaps of COFs provide them with remarkable efficiency for reactive oxygen species (ROS) generation, which has received considerable interest in photodynamic therapy (PDT) [12–19] and photocatalytic organic oxidations [20–22]. For instance, a corrole-based COF with evident absorption capability and high efficiency of singlet oxygen ($^1O_2$) generation has been proven to be outstanding in PDT [23]. Similarly, a glycosylated COF decorated with boron dipyrromethene (BODIPY) *via* post-synthetic modification has also displayed excellent performance in $^1O_2$ generation, leading to notable antitumor effect on the colon tumor *via* the synergistic therapy of PDT and $^1O_2$-triggered Ca^{2+} overload treatments [24]. Therefore, developing COFs in ROS-based PDT for tumor treatment is of great promise.

Generally, ROS consisting of oxygen-based free radicals and some non-radical derivatives of O_2, such as superoxide ($O_2^{\bullet-}$), $^1O_2$, hydroxyl radical ($^{\bullet}OH$), and hydrogen peroxide (H_2O_2), are vital for life on Earth, which work as cell signaling molecules for normal biological processes [25–31]. However, excessive generation of ROS could provoke oxidative stress that induces cell death through autophagy, apoptosis, and other signal pathways, leading to uncountable pathologies [32–34]. It is now well-established that a subtle but dynamic balance exists between ROS generation and the antioxidant defenses that maintain the health of living organisms [35,36]. Due to oxidative damage toward cells, ROS could also play a significant role in tumor treatment. Diverse studies have focused on rapidly producing high levels of ROS at tumor sites to cause local peroxidation of tumor cells, thereby promoting ROS damage to DNA, lipid and protein peroxidation, and mitochondrial depolarization in tumors, eventually achieving the effect of killing tumor cells [37–42]. Among ROS-based therapy, PDT is an effective method based on oxidation reactions, which could convert tissue O_2 into ROS by utilizing photosensitizers *via* light energy activation [43–47]. Compared with conventional therapy, PDT has numerous advantages over tumor treatment, including high tumor selectivity, low drug resistance, noninvasive nature, and devoid of side effects [48–52]. However, the therapeutic efficacy largely depends on the inherent capability to generate ROS.

* Corresponding authors.
E-mail addresses: mingcli@whu.edu.cn (M. Li), xianjunlang@whu.edu.cn (X. Lang).
[1] These authors contributed equally to this work.

https://doi.org/10.1016/j.cclet.2023.108564
1001-8417/

To this end, the generation of ROS over photoactive COFs could be accomplished in a biocompatible environment without transition metals and heavy elements. Our recent study demonstrates that a porphyrin COF (Por-DETH-COF) is an excellent amplifier of $O_2^{\bullet-}$, which could swiftly oxidize amines [53]. Nevertheless, the oxidation of amines proceeds *via* a nucleophilic attack pathway rather than direct oxidation. It would be more favorable to find direct and targeted oxidation for the generated ROS over Por-DETH-COF. Thiols are crucial components of many proteins and small molecules that play a vital role in maintaining redox homeostasis in living organisms [54,55]. Glutathione, the tripeptide thiol compound, is pervasive in cells of all organs, including the brain. Besides, glutathione is overexpressed in tumor chemical environments [56,57]. Therefore, the oxidation of thiol compounds is crucial in many biological processes [58]. Moreover, thiol compounds are highly reductive and could potentially impact the effectiveness of PDT, in which these thiol compounds are preferred to be partially eliminated. Fortunately, thiols could be directly oxidized by $O_2^{\bullet-}$ [59,60]. In addition, both $^1O_2$ and $O_2^{\bullet-}$ can be simultaneously generated over COFs and specifically used in oxidations [61,62].

Herein, a hydrazone-linked porphyrin COF Por-DETH-COF is constructed based on *p*-Por-CHO (*meso*-tetrakis(4-formylphenyl) porphyrin) and DETH (2,5-diethoxyterephthalohydrazide). Por-DETH-COF is employed for the generation of $^1O_2$ or $O_2^{\bullet-}$ to undertake different but targeted oxidations. First, $^1O_2$ is adopted in PDT for glioma treatment. Glioma is the most common primary malignant tumor of adult human central nervous system, accounting for 80% of all tumors [63], which can significantly affect the immune system with avoided apoptosis, unlimited cell growth, and enhanced transfer ability. Due to the existence of the blood-brain barrier, it is often difficult for drugs to reach tumors through blood circulation and aggregate sufficient concentration to achieve local therapeutic function. The PDT efficiency of Por-DETH-COF is explored to induce the apoptosis of glioma cells through flow cytometry and western blot assay. The results reveal that the apoptosis rate of glioma cells significantly increases over Por-DETH-COF under red light illumination, influencing the expression level of proapoptotic and anti-apoptosis-related proteins. Second, $O_2^{\bullet-}$ is employed for the targeted oxidation of thiols. The photocatalytic oxidation of thiols is used to mimic the effects of the generation of ROS over Por-DETH-COF under complex chemical environments. The results indicate that a series of thiols could be efficiently transformed into corresponding disulfides under red light illumination, confirming that Por-DETH-COF is a brilliant platform for ROS generation. This work highlights the great potential of COFs in ROS-based PDT applications under complex chemical environments.

Por-DETH-COF was constructed with *p*-Por-CHO and DETH according to our prior work [53] with some modifications (Supporting information and Scheme S1). Subsequently, powder X-ray diffraction (PXRD) and Fourier transform infrared (FTIR) spectra were collected to prove the successful construction of Por-DETH-COF. The crystallinity of Por-DETH-COF was determined by PXRD (Fig. 1a). The diffracted peaks around 3.0° and 6.1° were ascribed to the (110) and (220) facets, respectively. Additionally, other weak diffraction peaks at 4.3°, 9.0°, and 22.0° further demonstrated good crystallinity. Furthermore, the experimental PXRD pattern of Por-DETH-COF matched well with the calculated diffraction pattern with AA eclipsed stacking model in the prior report [64]. The hump centered at ~22.0° is probably indexed to zigzag π–π stacking of 2D layers [65]. FTIR spectra (Fig. 1b) were also gathered to analyze the characteristic functionalities of Por-DETH-COF. Due to the establishment of hydrazone linkage, the FTIR spectrum of Por-DETH-COF emerged with peaks at 1665 cm^{-1} and 1201 cm^{-1}. The observed band at around 3400 cm^{-1} was attributed to the –OH group of adsorbed water on Por-DETH-COF.

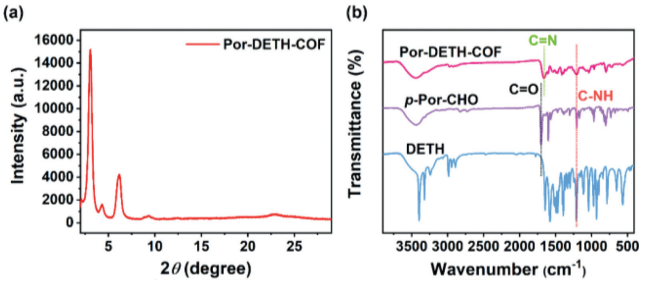

Fig. 1. (a) PXRD and (b) FTIR spectra of Por-DETH-COF, *p*-Por-CHO, and DETH.

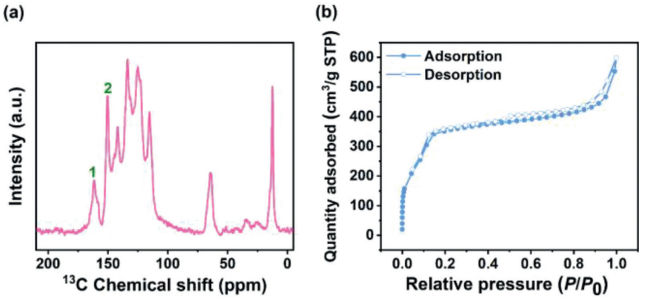

Fig. 2. (a) Solid-state ^{13}C NMR spectrum and (b) N_2 adsorption/desorption curve of Por-DETH-COF.

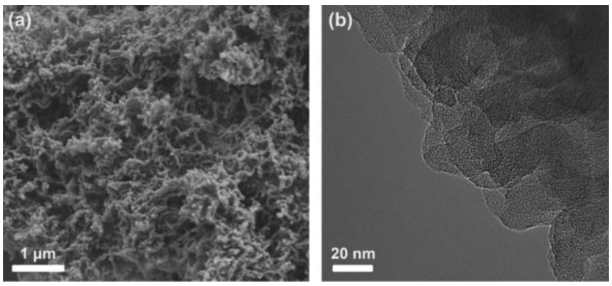

Fig. 3. (a) SEM and (b) TEM images of Por-DETH-COF.

Next, the construction of Por-DETH-COF was identified by solid-state ^{13}C nuclear magnetic resonance (NMR) spectroscopy. The ^{13}C resonance signal at ~162 ppm (marked 1) might be assigned to the hydrazone bond (Fig. 2a). The resonance signal at ~150 ppm (marked 2) was probably ascribed to the carbon of the C=N bond. The permanent porosity of the Por-DETH-COF was assessed by N_2 sorption analysis at 77 K, demonstrating a Brunauer–Emmett–Teller (BET) specific surface area of 925 m^2/g and a pore volume of 0.517 cm^3/g (Fig. 2b). The high specific surface area and large pore volume are conducive to the generation and diffusion of ROS over Por-DETH-COF, offering a brilliant platform for targeted oxidations.

Using scanning electron microscopy (SEM) and transmission electron microscopy (TEM), the morphology of Por-DETF-COF was investigated (Figs. 3a and b). Por-DETF-COF was composed of stacked and interwoven network structures. The solid-state UV–visible spectrum of Por-DETH-COF exhibited a wide absorption edge around 400–700 nm (Fig. 4a). Based on the Kubelka–Munk function, the bandgap (E_g) of Por-DETH-COF was roughly estimated at 1.75 eV from the absorption edge (Fig. 4b). In principle, the E_g of Por-DETH-COF is narrow enough to efficiently harvest visible light. Namely, it is well-founded to realize red light-induced generation of ROS over Por-DETH-COF. Red light is essential for biomedical applications because it can penetrate cells more efficiently.

The electron paramagnetic resonance (EPR) spectra of Por-DETH-COF were collected. Compellingly, Por-DETH-COF is a brilliant platform for ROS generation. According to EPR results

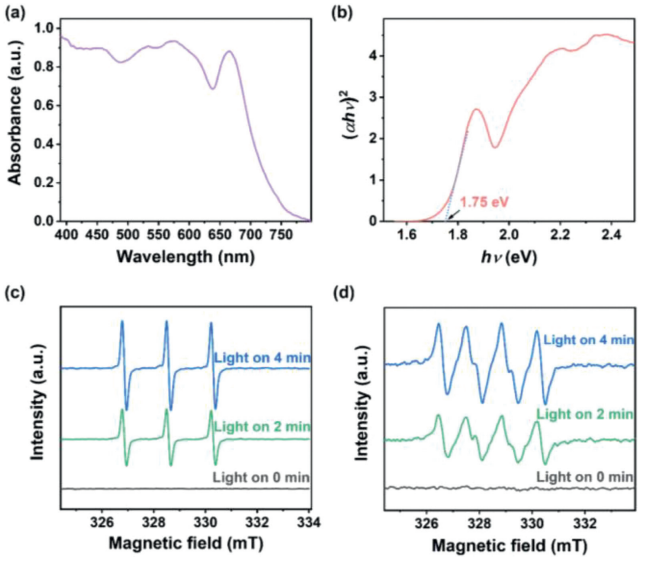

Fig. 4. (a) Solid-state UV–visible spectrum and (b) E_g of Por-DETH-COF calculated by the Kubelka–Munk formula. The collected EPR spectra of (c) $^1O_2$ captured by TMPD and (d) $O_2^{\bullet-}$ captured by DMPO over Por-DETH-COF under red light illumination.

(Fig. 4c), the signal of $^1O_2$ trapped by 2,2,6,6-tetramethyl-4-piperidone (TMPD) was generated and enhanced with red light illumination, implying that $^1O_2$ is produced under red light illumination through an energy transfer pathway [66]. Moreover, the production of $O_2^{\bullet-}$ was also confirmed, whose EPR signal was displayed by 5,5-dimethyl-1-pyrroline *N*-oxide (DMPO). The signal of DMPO-$O_2^{\bullet-}$ adducts was noticeable under red light illumination and increased with time of illumination (Fig. 4d), which evidences the efficient generation of $O_2^{\bullet-}$. By and large, two types of ROS, namely $^1O_2$ and $O_2^{\bullet-}$, could be sufficiently generated over Por-DETH-COF under 660 nm red light illumination.

After confirming the capability of ROS generation over Por-DETH-COF, the generated $^1O_2$ over Por-DETH-COF was applied in tumor treatments. Glioma cells were first taken as the targeted oxidation over Por-DETH-COF. The GBM cell lines (U87) were purchased from the American Type Culture Collection (ATCC). These cells were cultured at 37 °C with 5% CO_2 in Dulbecco's modified Eagle's medium, 10% fetal bovine serum (Gibco), and 1% penicillin/streptomycin (4 mg/mL; Sigma Aldrich). Experiments were conducted at a cell density of 70%–80%. Antibodies against B-cell lymphoma-2 (Bcl-2), Bcl-2-Associated X (Bax), Cleaved Caspase-3 (CC3), and glyceral-dehyde-3-phosphate dehydrogenase (GAPDH) were purchased from Cell Signaling Technology (Beverly, USA). Glioma cells and red light-emitting diodes (LEDs) ($\lambda = 660 \pm 8$ nm) were used as target object and light source, respectively. Flow cytometry showed the effect of red light illumination over Por-DETH-COF on the apoptosis of glioma cells. The results showed that after adding Por-DETH-COF to the sample along with illumination of red light for 24 h, the apoptosis rate of glioma cells significantly increased in light + Por-DETH-COF group, which is substantially higher than that of the control group, light group, and Por-DETH-COF group ($P < 0.05$). The apoptosis rate slightly increased in the light group and the Por-DETH-COF group compared with the control group (Figs. 5a and b).

In addition, western blot assay was used to detect the expression level of glioma-related proteins. Western blot analysis was performed as described in Supporting information. It showed that compared with the control group, light group, and Por-DETH-COF group, the expression level of proapoptotic-related proteins Bax and CC3 was significantly increased, while the expression level of anti-apoptosis-related protein Bcl-2 was considerably suppressed in light + Por-DETH-COF group (Figs. 5c and d). Meanwhile, only a slight increase in apoptosis was observed in the light group and the Por-DETH-COF group. The Western blot results showed that Por-DETH-COF under red light illumination could significantly induce the apoptosis of glioma cells and inhibit the growth of glioma cells, which is consistent with flow cytometry results. However, one should not take it for granted that the apoptosis of glioma cells was solely caused by PDT of $^1O_2$ over Por-DETH-COF. Glioma cells live alongside complex cellular chemical environments, which could impact the effectiveness of ROS.

Next, Por-DETH-COF was then applied to the targeted oxidation of thiols. Notably, the red light-induced oxidation of 4-methoxybenzenethiol smoothly occurred in an atmosphere of O_2

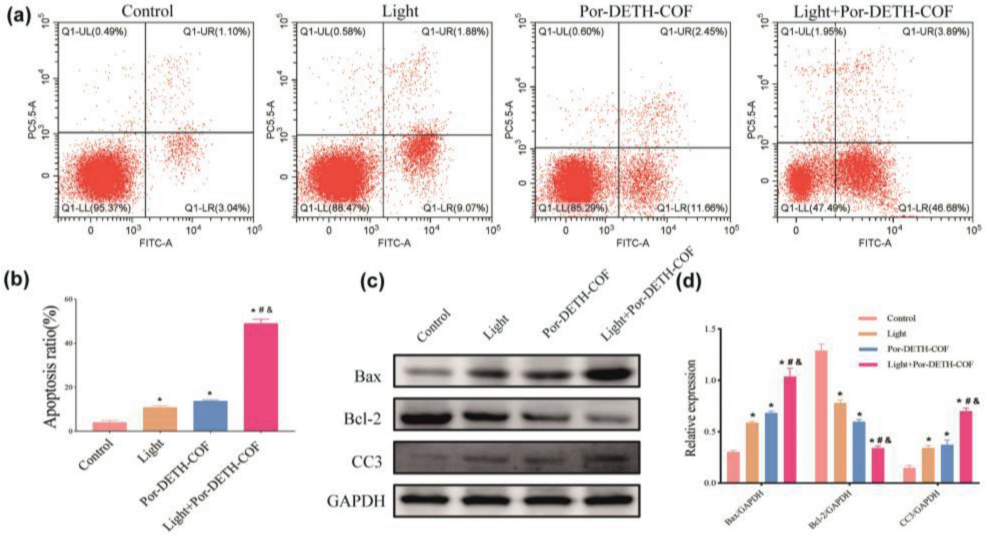

Fig. 5. Red light-induced apoptosis of glioma cells (U87) *in vitro* over Por-DETH-COF. (a and b) Apoptosis assay analysis by flow cytometry of glioma U87 cells in the control group, light group, Por-DETH-COF group, and light + Por-DETH-COF group. (c and d) Cell apoptosis-related protein expression quantified with western blot. The light group represents red light illumination without adding the Por-DETH-COF group; The Por-DETH-COF group represents adding Por-DETH-COF without red light illumination group; Light + Por-DETH-COF group represents the Por-DETH-COF with red light illumination group. * represents $P < 0.05$ compared with the control group, # represents $P < 0.05$ compared with the light group, and & represents $P < 0.05$ compared with the Por-DETH-COF group.

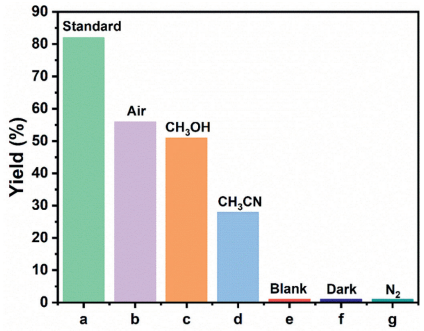

Fig. 6. Control experiments for the red light-induced oxidation of thiols over Por-DETH-COF. Standard reaction conditions: Por-DETH-COF (5 mg), 4-methoxybenzenethiol (0.3 mmol), O_2 (1 atm), C_2H_5OH (1 mL), red LEDs (660 ± 8 nm), 0.5 h.

(Fig. 6, bar a). Additionally, the production of disulfide was also possible under air (Fig. 6, bar b). In comparison, the yield of disulfide benefited from the improved O_2 pressure. As observed, it was practical but less effective when C_2H_5OH was replaced by CH_3OH or CH_3CN (Fig. 6, bars c and d). Moreover, the functions of the rest components of the system were also studied. Under comparable conditions, self-oxidation under red light illumination could not be completed when only 4-methoxybenzenethiol existed (Fig. 6, bar e). In contrast to the experiment performed in the dark, where no products were formed, thiol conversion equally did not occur when O_2 was removed by N_2 (Fig. 6, bars f and g). Por-DETH-COF, O_2, and light source were all essential for this system, confirming the suspicions that the oxidation is induced by activating O_2 to proper ROS over Por-DETH-COF under red light illumination. Deutered solvent could prolong the lifetime of $^1O_2$, which in turn could improve the conversion. Notwithstanding, the photocatalytic conversion of 4-methoxybenzenethiol was not improved when C_2H_5OH was replaced by C_2D_5OD, suggesting that $^1O_2$ does not partake in the oxidation of thiol and $O_2^{\bullet-}$ is the pivotal ROS.

To verify the universality, a series of thiols were investigated as the substrates for photocatalytic oxidation over Por-DETH-COF (Table 1). In comparison with benzenethiol, electron-donating derivatives were smoothly converted into corresponding disulfides with less reaction time (Table 1, entries 1–4). As for electron-withdrawing groups like −F, −Cl, and −Br substituted thiols, the rate of transformation was comparable to that of benzenethiol (Table 1, entries 7–9). However, 4-(trifluoromethyl)benzenethiol suffered from decreased conversion for the stronger electron-withdrawing effect of $-CF_3$ (Table 1, entry 10). For comparison, the performances of the same substituent ($-OCH_3$) at different positions on targeted oxidation of thiols were displayed (Table 1, entries 4–6). It was shown that the steric effect could partly inhibit the effective conversion of thiols. Under red light illumination, Por-DETH-COF induced the efficient conversion of various thiols and enabled the generation of disulfides with $O_2^{\bullet-}$.

Eventually, a mechanism for the targeted oxidation of benzenethiol over Por-DETH-COF is proposed in Fig. 7. Initially, Por-DETH-COF is excited by red light illumination, resulting in the separation of electron (e^-) and hole (h^+). Then e^- combines with O_2 to generate $O_2^{\bullet-}$. Benzenethiol is activated by $O_2^{\bullet-}$ and converted to a sulfur-centered radical. The sulfur-centered radical couples with another benzenethiol, forming a disulfide and releasing hydrogen radical ($H^{\bullet}$). For the steady generation of $O_2^{\bullet-}$, the h^+ should be partially quenched by $H^{\bullet}$ to release H^+. The released H^+ reacts with the $O_2^{\bullet-}$, which is eventually converted to H_2O_2.

In summary, Por-DETH-COF has been successfully developed as a platform for ROS generation to undertake targeted oxidations. Firstly, the PDT efficiency of the generated $^1O_2$ over Por-DETH-

Table 1
Red light-induced photocatalytic oxidation of thiols into disulfides over Por-DETH-COF.[a]

Entry	Substrate	Product	*t* (h)	Conv. (%)[b]	Sel. (%)[b]
1		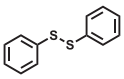	1.2	89	99
2		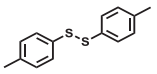	0.9	90	99
3	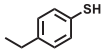	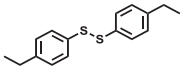	1.0	90	99
4	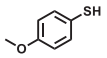	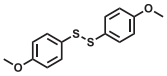	0.7	94	99
5	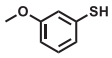	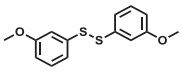	1.3	90	99
6		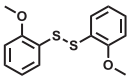	1.7	80	99
7		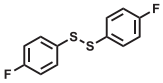	1.2	85	99
8		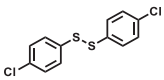	1.2	87	99
9		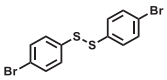	1.2	90	99
10		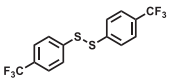	1.5	73	99

[a] Reaction conditions: Por-DETH-COF (5 mg), thiol (0.3 mmol), O_2 (1 atm), C_2H_5OH (1 mL), red LEDs (660 ± 8 nm).
[b] Determined by GC–FID using chlorobenzene as the internal standard, conversion of thiol, and selectivity of corresponding disulfide.

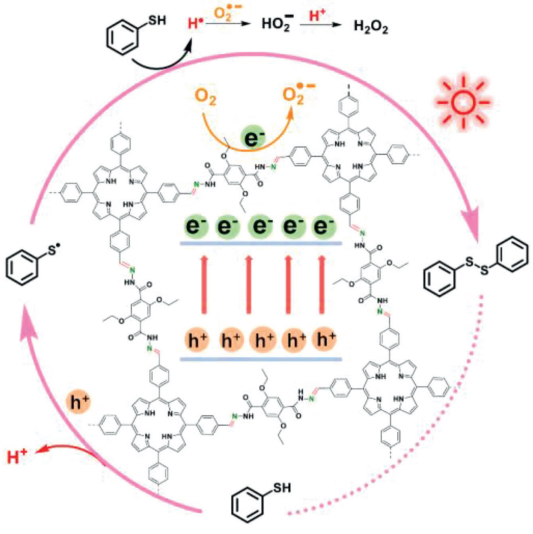

Fig. 7. A proposed mechanism of the red light-induced generation of $O_2^{\bullet-}$ over Por-DETH-COF for the targeted oxidation of thiol.

COF was explored on the apoptosis of glioma cells through flow cytometry and western blot assay. The results revealed that Por-DETH-COF significantly increased the apoptosis rate of glioma cells under red light illumination by influencing the expression level of proapoptotic and anti-apoptosis-related proteins. Second, the effectiveness of the afforded $O_2^{\bullet-}$ over Por-DETH-COF was assessed by the photocatalytic oxidation of thiols. A series of thiols could be efficiently transformed into corresponding disulfides under red light illumination. Overall, Por-DETH-COF is a brilliant platform for ROS generation. This work highlights the great potential of COFs in generating ROS for precise medical applications of complex chemical environments.

Declaration of competing interest

The authors declare that they have no known competing financial interests or personal relationships that could have appeared to influence the work reported in this paper.

Acknowledgment

This work was supported by the National Natural Science Foundation of China (No. 22072108). We also acknowledge the Core Facility of Wuhan University for materials characterizations.

Supplementary materials

Supplementary material associated with this article can be found, in the online version, at doi:10.1016/j.cclet.2023.108564.

References

[1] T. Zhang, G. Zhang, L. Chen, Acc. Chem. Res. 55 (2022) 795–808.
[2] Y.F. Zhi, P.P. Shao, X. Feng, et al., J. Mater. Chem. A 6 (2018) 374–382.
[3] L.P. Guo, J. Zhang, Q. Huang, et al., Chin. Chem. Lett. 33 (2022) 2856–2866.
[4] S.H. Wu, Y. Pan, H. Lin, et al., ChemSusChem 14 (2021) 4958–4972.
[5] H.X. Lin, C.P. Chen, T.H. Zhou, et al., Sol. RRL 2 (2021) 2000458.
[6] Y. Xie, Y.L. Chen, X. Sun, et al., Chin. Chem. Lett. 32 (2021) 2061–2065.
[7] S.M. Li, J. Zou, L.F. Tan, et al., Chem. Eng. J. 446 (2022) 137148.
[8] S. Bhunia, K.A. Deo, A.K. Gaharwar, Adv. Funct. Mater. 30 (2020) 2002046.
[9] Y.L. Zheng, S.N. Zhang, J.B. Guo, et al., Angew. Chem. Int. Ed. 61 (2022) e202208744.
[10] Q. Sun, B. Aguila, P.C. Lan, et al., Adv. Mater. 31 (2019) 1900008.
[11] G.Y. Zhang, X.L. Li, Q.B. Liao, et al., Nat. Commun. 9 (2018) 2785.
[12] J. Tian, B.X. Huang, M.H. Nawaz, et al., Coord. Chem. Rev. 420 (2020) 213410.
[13] D.W. Wang, Z. Zhang, L. Lin, et al., Biomaterials 223 (2019) 119459.
[14] F. Lu, L.M. Pan, T. Wu, et al., Chem. Commun. 58 (2022) 11013–11016.
[15] L. Zhang, Y. Xiao, Q.C. Yang, et al., Adv. Funct. Mater. 32 (2022) 2201542.
[16] A.R. Bagheri, C.J. Li, X.L. Zhang, et al., Biomater. Sci. 9 (2021) 5745–5761.
[17] S.N. Liu, Z.D. Liu, Q. Meng, et al., ACS Appl. Mater. Interfaces 13 (2021) 56873–56880.
[18] P. Gao, M.Z. Wang, Y.Y. Chen, et al., Chem. Sci. 11 (2020) 6882–6888.
[19] S. Chen, T.T. Sun, M. Zheng, et al., Adv. Funct. Mater. 30 (2020) 2004680.
[20] H.M. Hao, F.L. Zhang, X.Y. Dong, et al., Appl. Catal. B 299 (2021) 120691.
[21] X. Li, S.X. Yang, F.L. Zhang, et al., Appl. Catal. B 303 (2022) 120846.
[22] J.Y. Guo, D.G. Ma, F.L. Sun, et al., Sci. China Chem. 65 (2022) 1704–1709.
[23] Y.M. Zhao, W.H. Dai, Y.L. Peng, et al., Angew. Chem. Int. Ed. 59 (2020) 4354–4359.
[24] Q. Guan, L.L. Zhou, F.H. Lv, et al., Angew. Chem. Int. Ed. 59 (2020) 18042–18047.
[25] R.P. Ostrowski, E.B. Pucko, Neurochem. Int. 154 (2022) 105281.
[26] S. Liu, L. Dong, W. Shi, et al., Front. Pharmacol. 13 (2022) 921070.
[27] S. George, M.R. Hamblin, H. Abrahamse, J. Photochem. Photobiol. B 188 (2018) 60–68.
[28] K.B. Mollers, H. Mikkelsen, T.I. Simonsen, et al., Carbohydr. Res. 448 (2017) 182–186.
[29] X.X. Ren, H. Liu, X.M. Wu, et al., Front. Bioeng. Biotechnol. 9 (2022) 820468.
[30] L. Luo, T.T. Zhang, M. Wang, et al., ChemSusChem 13 (2020) 5173–5184.
[31] H. Li, X. Li, J. Zhou, et al., Chin. Chem. Lett. 33 (2022) 3733–3738.
[32] B.W. Yang, Y. Chen, J.L. Shi, Chem. Rev. 119 (2019) 4881–4985.
[33] H. Sies, D.P. Jones, Nat. Rev. Mol. Cell Biol. 21 (2020) 363–383.
[34] B.M. Scavuzzi, J. Holoshitz, Antioxidants 11 (2022) 1306.
[35] X.Q. Hu, D.L. Dong, M.H. Xia, et al., New J. Chem. 44 (2020) 11405–11419.
[36] T. Liu, L. Sun, Y.B. Zhang, et al., J. Biochem. Mol. Toxicol. 36 (2022) e22942.
[37] M. Ismail, W. Yang, Y. Li, et al., Biomaterials 289 (2022) 121760.
[38] S.Y. Liu, Z.L. Zhong, C.W. Zhang, et al., Nanoscale Adv. 4 (2022) 894–903.
[39] A. Xie, H. Li, Y.M. Hao, et al., Nanoscale Res. Lett. 16 (2021) 142.
[40] Q. Guan, L.L. Zhou, Y.A. Li, et al., ACS Nano 13 (2019) 13304–13316.
[41] Z.J. Zhang, L. Wang, W.X. Liu, et al., Natl. Sci. Rev. 8 (2021) nwaa155.
[42] S. Malekkhaiat Häffner, E. Parra-Ortiz, M.W.A. Skoda, et al., J. Colloid Interface Sci. 584 (2021) 19–33.
[43] Y. Nosaka, A.Y. Nosaka, Chem. Rev. 117 (2017) 11302–11336.
[44] F.M. Wei, T.W. Rees, X.X. Liao, et al., Coord. Chem. Rev. 432 (2021) 213714.
[45] H. Huang, W. Feng, Y. Chen, Chem. Soc. Rev. 50 (2021) 11381–11485.
[46] W.H. Sun, Y.G. Xiang, Z.H. Jiang, et al., Sci. Bull. 67 (2022) 61–70.
[47] Y.C. Zhang, L. She, Z.Y. Xu, et al., Chin. Chem. Lett. 33 (2022) 3277–3280.
[48] M.Y. Yang, T. Yang, C.B. Mao, Angew. Chem. Int. Ed. 58 (2019) 14066–14080.
[49] M. Pan, Q.Y. Jiang, J.L. Sun, et al., Angew. Chem. Int. Ed. 59 (2020) 1897–1905.
[50] X.J. He, B. Situ, M. Gao, et al., Small 15 (2019) 1905080.
[51] L.G. Yu, Q. Wang, R.C.H. Wong, et al., Dyes Pigm. 163 (2019) 197–203.
[52] C.L. Wu, Y.Y. Li, Z.H. Cheng, et al., Chin. Chem. Lett. 33 (2022) 4339–4344.
[53] S.J. Wu, Y.F. Zhang, H.M. Ding, et al., J. Colloid Interface Sci. 610 (2022) 446–454.
[54] Y.L. Luo, B. Cao, M.J. Zhong, et al., Angew. Chem. Int. Ed. 61 (2022) e2022126.
[55] C.H. Foyer, Environ. Exp. Bot. 154 (2018) 134–142.
[56] L.L. Feng, B. Liu, R. Xie, et al., Adv. Funct. Mater. 31 (2021) 2006216.
[57] H.J. Zhang, R.L. Han, P.X. Song, et al., J. Colloid Interface Sci. 629 (2023) 103–113.
[58] D. Schilter, Nat. Rev. Chem. 1 (2017) 0013.
[59] H. Xu, Y.F. Zhang, X.J. Lang, Chin. Chem. Lett. 31 (2020) 1520–1524.
[60] X.B. Li, Z.J. Li, Y.J. Gao, et al., Angew. Chem. Int. Ed. 53 (2014) 2085–2089.
[61] F.L. Zhang, X.M. Ma, X.Y. Dong, et al., Chem. Eng. J. 451 (2023) 138802.
[62] S.X. Yang, X. Li, Y. Qin, et al., ACS Appl. Mater. Interfaces 13 (2021) 29471–29481.
[63] Q.T. Ostrom, L. Bauchet, F.G. Davis, et al., Neuro-oncology 16 (2014) 896–913.
[64] R.F. Chen, Y. Wang, Y. Ma, et al., Nat. Commun. 12 (2021) 1354.
[65] Z.X. Lu, Y.X. Liu, X.L. Liu, et al., J. Mater. Chem. B 7 (2019) 1469–1474.
[66] Y.J. Fu, M. Tan, Z.L. Guo, et al., Chem. Eng. J. 452 (2023) 139417.